Supplementary Materials

Surface-Hydrogenation Activity Regulation toward Robust Anti-Poisoning of ZrCo-based Hydrogen Isotope Storage Materials

Qianwen Zhou [a], Yiting Yu [a], Panpan Zhou [a, c, *], Shunrui Xiao [a], Jingyu Hu [a], Xuezhang Xiao [a, d, *], Xingwen Feng [e], Huaqin Kou [e, *], Wenhua Luo [e], Xiulin Fan [a, *], Lixin Chen [a, b, f, *]

[a] *State Key Laboratory of Silicon and Advanced Semiconductor Materials; School of Materials Science and Engineering, Zhejiang University, Hangzhou 310058, Zhejiang, China*

[b] *Institute of Wenzhou, Zhejiang University, Wenzhou 325006, China*

[c] *College of Materials Science and Engineering, Hohai University, Changzhou 213200, Jiangsu, China*

[d] *School of Advanced Energy, Sun Yat-sen University (Shenzhen), Shenzhen 518107, Guangdong, China*

[e] *Institute of Materials, China Academy of Engineering Physics, Mianyang 621907, Sichuan, China*

[f] *Key Laboratory of Hydrogen Storage and Transportation Technology of Zhejiang Province, Hangzhou 310027, Zhejiang, China*

** Corresponding author.*

Email: lxchen@zju.edu.cn (L.X. Chen), xlfan@zju.edu.cn (X.L. Fan), ppzhou@hhu.edu.cn (P.P. Zhou), xiaoxzh6@mail.sysu.edu.cn (X.Z. Xiao), kouhuaqin@caep.cn (H.Q. Kou)

Experimental

Sample preparation

The $ZrCo_{1-x}V_x$ (x = 0, 0.01, 0.03, 0.05, 0.1) and $Zr_{0.9}V_{0.1}Co$ alloys in this work were synthesized by induction levitation melting (ILM). High purity Zirconium (Zr, 99.9%), Cobalt (Co, 99.9%), and Vanadium (V, 99.9%) were used without further purification. The melting process of the ingots was carried out in a water-cooled copper crucible under a high-purity argon atmosphere (99.99%). To ensure the uniformity of elements and phases, each ingot was flipped and remelted three times. Subsequently, the surface of the as-melted ingots was polished to remove the oxide layer. The ingots were then placed in a stainless-steel milling tank and subjected to dynamic vacuuming for 30 min, followed by hydrogenation and pulverization under 40 bar of hydrogen pressure for 12 h. Finally, the hydrogenated and pulverized hydride powders were stored in a high-purity argon-filled glove box for subsequent characterization and hydrogen storage property measurements.

Materials characterizations

Phase structures of as-activated, after-dehydrogenation $ZrCo_{1-x}V_x$ (x = 0, 0.01, 0.03, 0.05, 0.1) and $Zr_{0.9}V_{0.1}Co$ alloys were examined by X-ray diffraction (XRD, PANalytical) using Cu Kα radiation. Phase abundance and lattice parameters were determined through Rietveld refinement performed with the FullProf Suite program. Microstructural features and elemental distributions were examined using a scanning electron microscope (SEM, HITACHI SU8600, operated at 3.0 kV) and transmission electron microscopy (TEM, Tecnai TF200, operated at 200 kV).

Hydrogen storage property measurements

Hydrogen storage properties in this study were measured using a custom-built Sieverts-type apparatus. For each test, 0.5 g of hydrogenated alloy powder was

loaded into a stainless-steel reactor and dehydrogenated under dynamic vacuum at 550 °C for 1 h. Hydrogenation kinetics were then measured at room temperature under 4 bar H_2, using either pure hydrogen or a hydrogen-based mixed gas containing 5000 ppm CO. To suppress the disproportionation tendency of the ZrCo alloy during cycling property measurements, the sample was held at 550 °C for 1 h to achieve complete reverse disproportionation. It was then cooled to room temperature (20 °C) and hydrogenated under a mixed gas atmosphere.

DFT calculations

To investigate the effects of different V substitution strategies on the CO adsorption behavior on the surface of ZrCo-based hydrogen isotope storage materials, this study employed first-principles density functional theory (DFT) calculations using the Vienna Ab-initio Simulation Package (VASP) along with the projector augmented wave (PAW) method [1-3]. The Perdew-Burke-Ernzerhof (PBE) functional within the generalized gradient approximation (GGA) was adopted to treat electron correlation effects [4-8]. During geometry optimization, the plane-wave cutoff energy was set to 550 eV, with convergence criteria of 0.01 eV/Å for atomic forces and 10^{-6} eV for total energy. To evaluate the changes in unit cell dimensions induced by elemental doping and the resulting local strain effects, the atomic substitution sites were divided into Zr sites and Co sites (as shown in Fig. S2). Structural calculations were performed using a 2×2×2 ZrCo supercell model, with single-element substitution resulting in alloy compositions of either $Zr_{0.875}M_{0.125}Co$ or $ZrCo_{0.875}M_{0.125}$, respectively. To verify the reliability of the DFT calculations, the lattice parameters of the ZrCo alloy were calculated after structural relaxation, yielding $a = b = c = 3.174$ Å. To investigate the adsorption behavior of gas molecules on the ZrCo surface, a 3×2 supercell of the ZrCo (110) surface was constructed based on previous research [9-11], and a vacuum layer of 15 Å was added to minimize periodic interactions. The adsorption energy of gas on the ZrCo (110) surfaces can be obtained by follow:

$E_{ads} = E_{slab+gas} - E_{slab} - E_{gas}$, where $E_{slab+gas}$, E_{slab} and E_{gas} are the energies of the adsorption system, the surface, and the adsorbed species, respectively. Besides, a 3×3×1 Γ-centered k-point mesh was adopted. To further analyze the electronic interactions between CO and the V-substituted ZrCo alloys, as well as the C-O bond strength, the projected density of states (PDOS) and crystal orbital Hamiltonian population (COHP) were also evaluated [12-14]. All structural and electronic visualizations were generated using the VESTA software.

Supplementary Figures

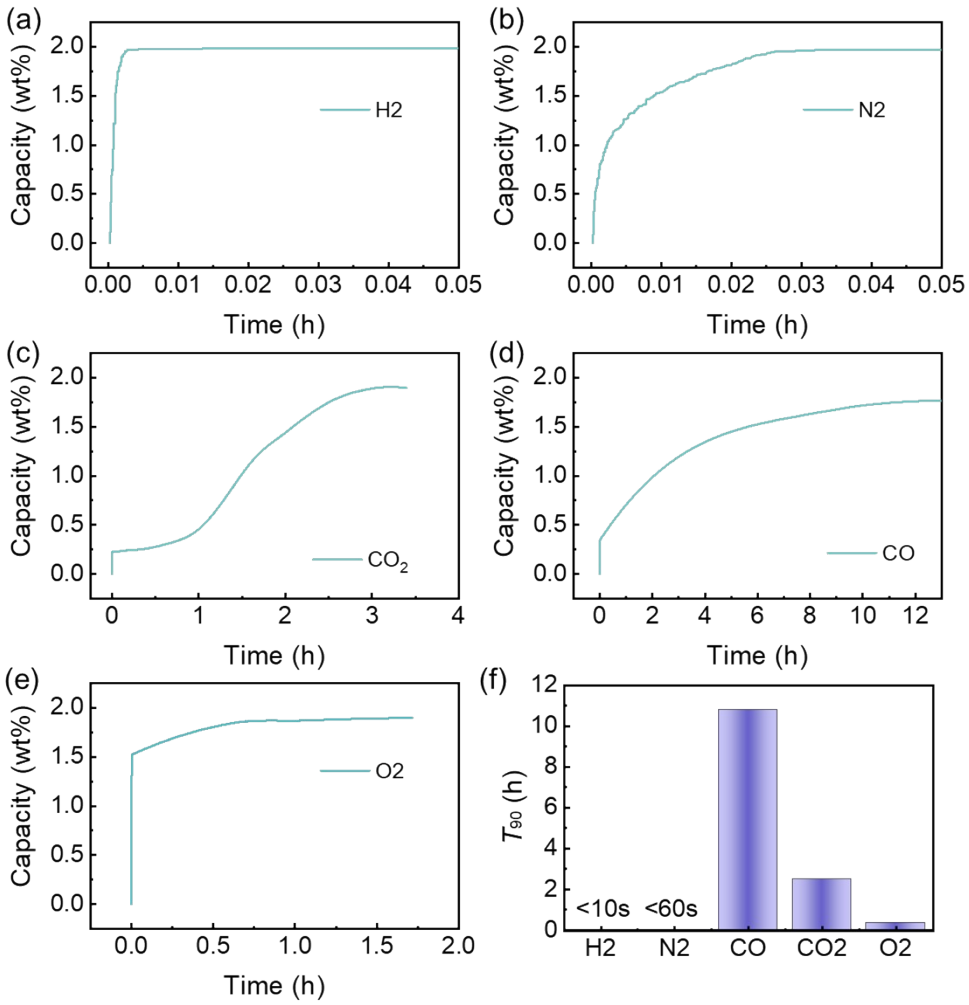

Fig. S1. Hydrogenation kinetics of ZrCo alloy in 4 bar (a) pure H_2, (b)H_2 + 5000 ppm N_2, (c)H_2 + 5000 ppm CO_2, (d)H_2 + 5000 ppm CO, (e)H_2 + 5000 ppm O_2, and (f) corresponding *T*90 (the time for 90% capacity).

Sc	Ti	V	Cr	Mn	Fe	**Co**	Ni	Cu
Y	**Zr**	Nb	Mo	Tc	Ru	Rh	Pd	Ag
La	Hf	Ta	W	Re	Os	Ir	Pt	Au

Fig. S2. Atomic substitution sites for Zr or Co sites according previous research (Zr side substitution elements marked in red and Co side substitution elements marked in blue).

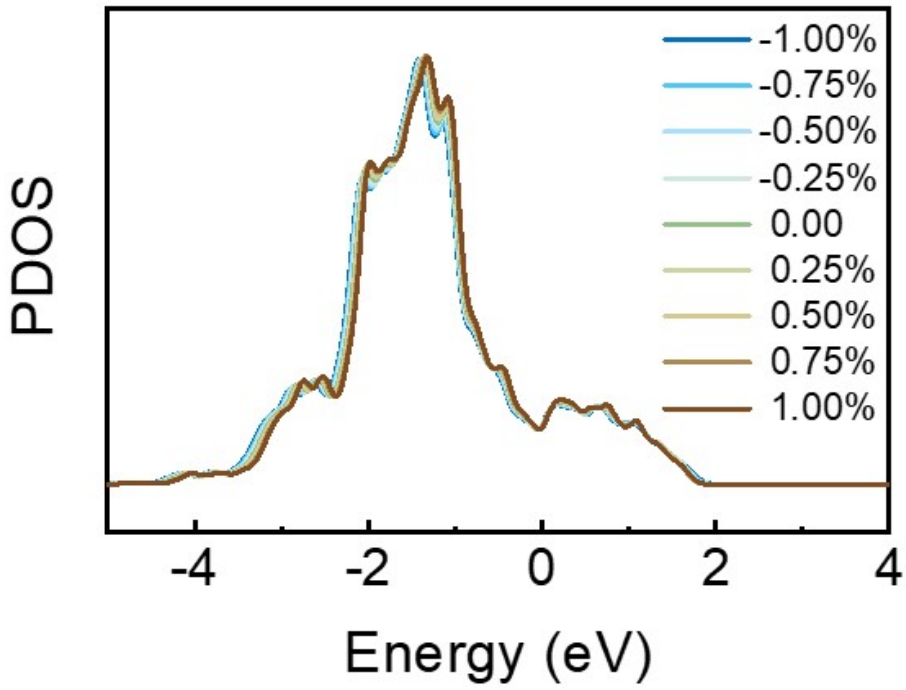

Fig. S3. Modulation of PDOS of the ZrCo (110) surface by crystal strain.

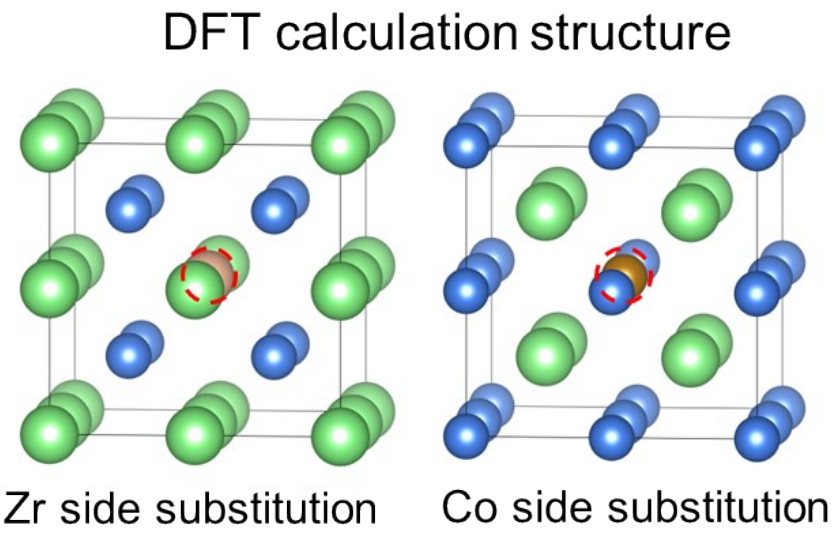

Fig. S4. The DFT calculation structure for the positions of the dopant atoms.

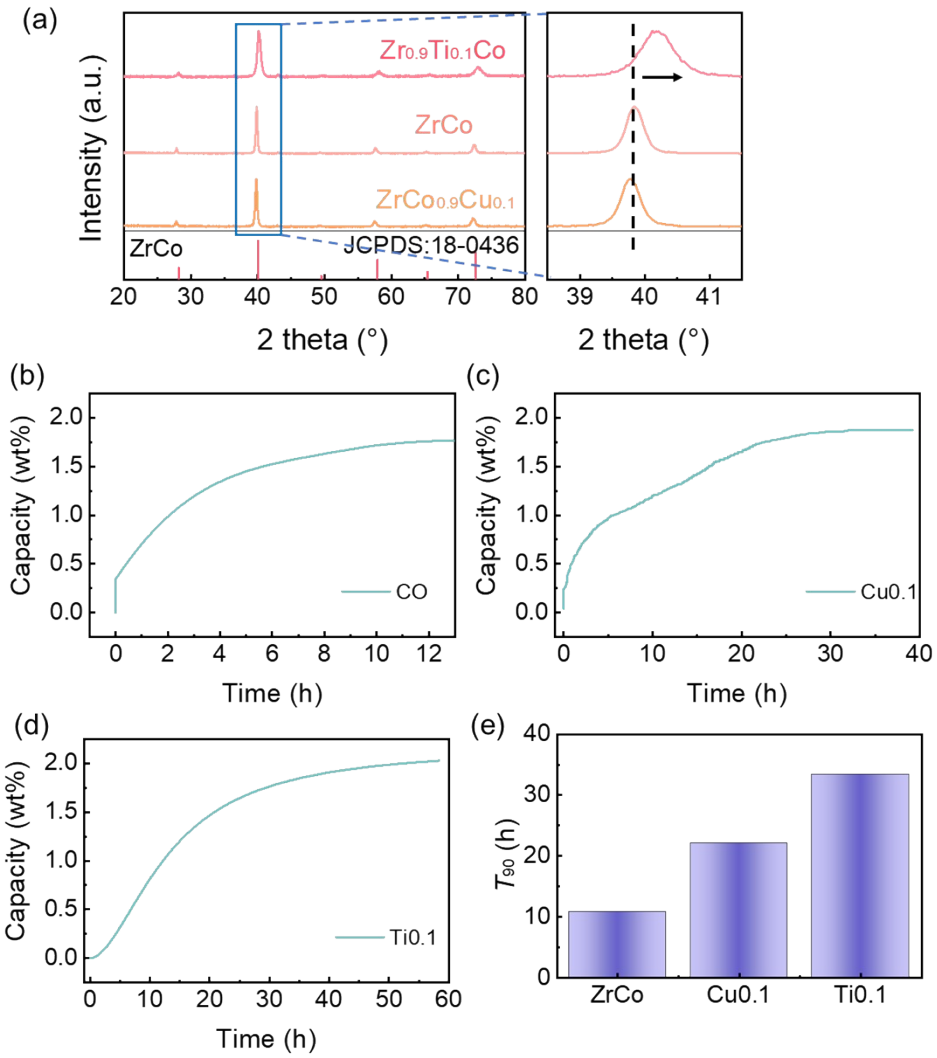

Fig. S5. (a) XRD patterns and local magnifications of the comparative of $Zr_{0.9}Ti_{0.1}Co$ and $ZrCo_{0.9}Cu_{0.1}$ alloy samples. Hydrogenation kinetics of (b) ZrCo, (c)$ZrCo_{0.9}Cu_{0.1}$ and (d) $Zr_{0.9}Ti_{0.1}Co$ alloy in 4 bar H_2 + 5000 ppm CO. (e) corresponding *T*90 (the time for 90% capacity)

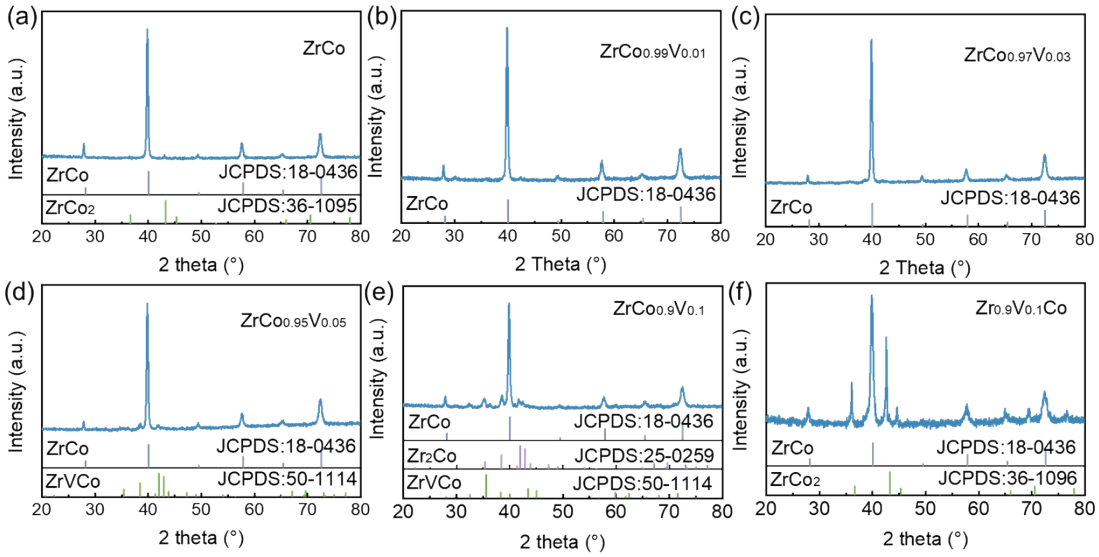

Fig. S6. XRD patterns of $ZrCo_{1-x}V_x$ (x= 0, 0.01, 0.03, 0.05, 0.1) and $Zr_{0.99}V_{0.01}Co$ alloys.

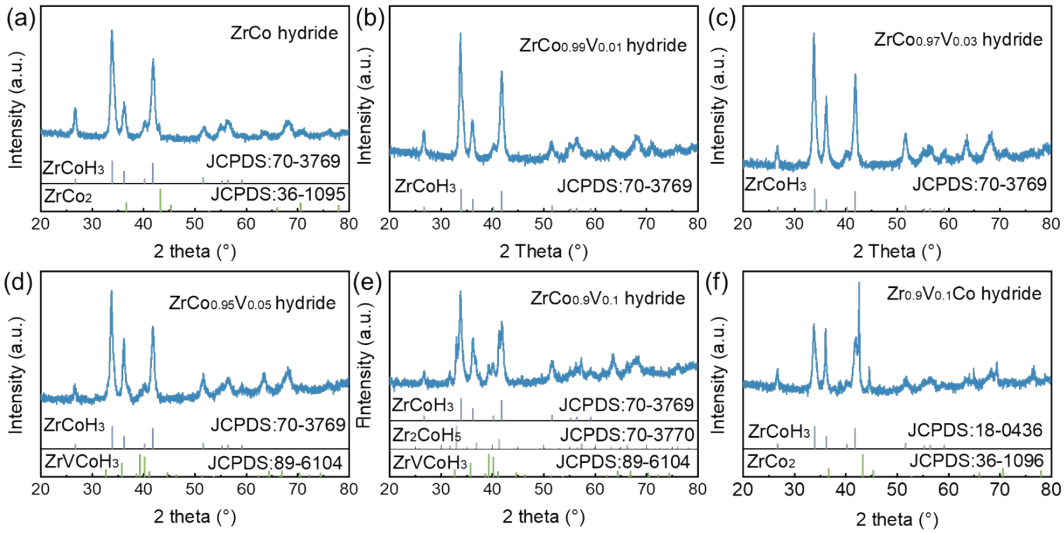

Fig. S7. XRD patterns of $ZrCo_{1-x}V_x$ (x = 0, 0.01, 0.03, 0.05, 0.1) and $Zr_{0.99}V_{0.01}Co$ hydrides.

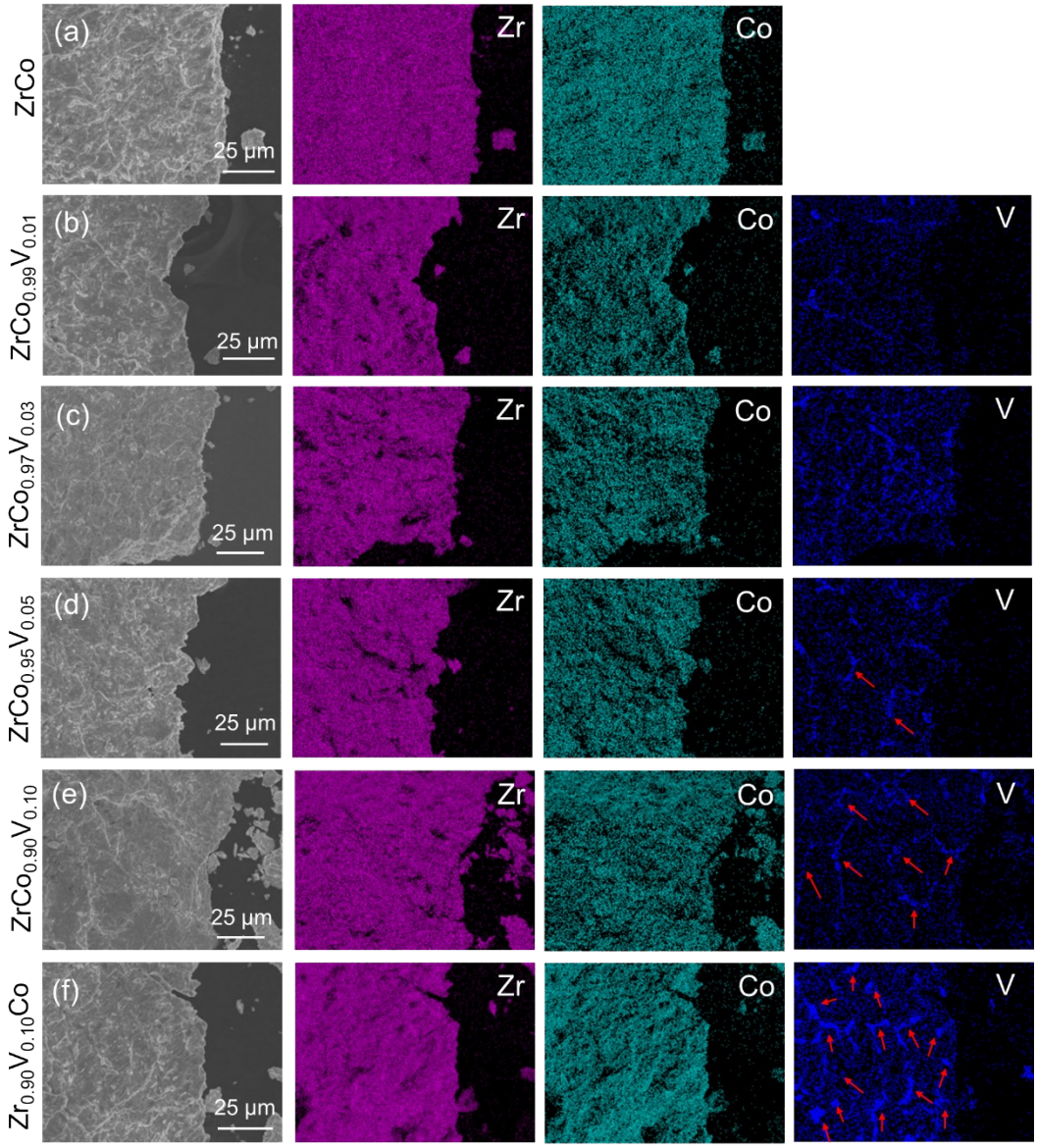

Fig. S8. SEM micrographs of $ZrCo_{1-x}V_x$ (x= 0, 0.01, 0.03, 0.05, 0.1) and $Zr_{0.90}V_{0.1}Co$ particles and their corresponding EDS mapping for Zr, Co, V elements.

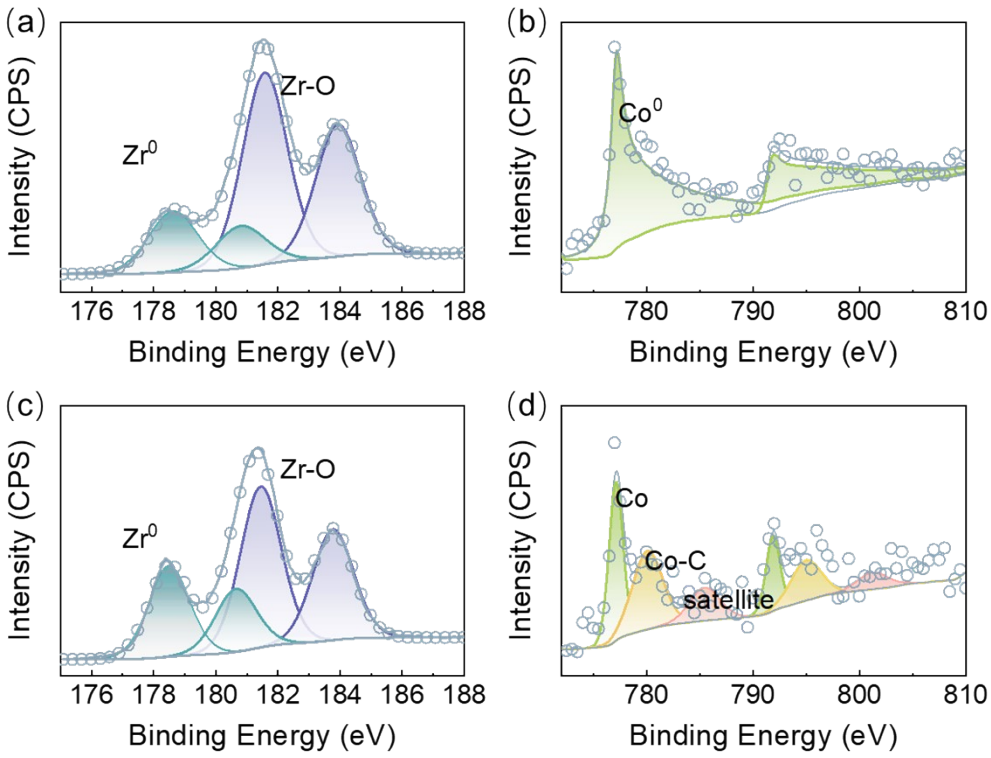

Fig. S9. (a) Zr 3d and (b) Co 2p XPS spectra of $ZrCo_{0.97}V_{0.03}$ alloy before cycle. (c) Zr 3d and (d) Co 4d XPS spectra of $ZrCo_{0.97}V_{0.03}$ alloy after cycle in H_2+5000 ppm CO.

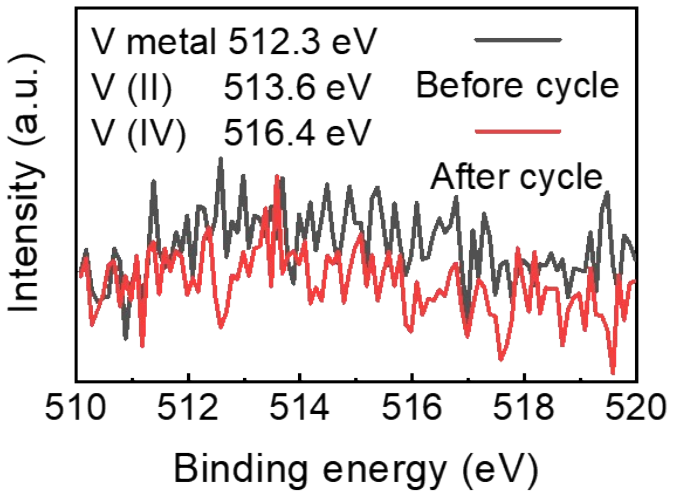

Fig. S10. V 2p XPS spectra of $ZrCo_{0.97}V_{0.03}$ alloy before and after cycle in H_2+5000 ppm CO.

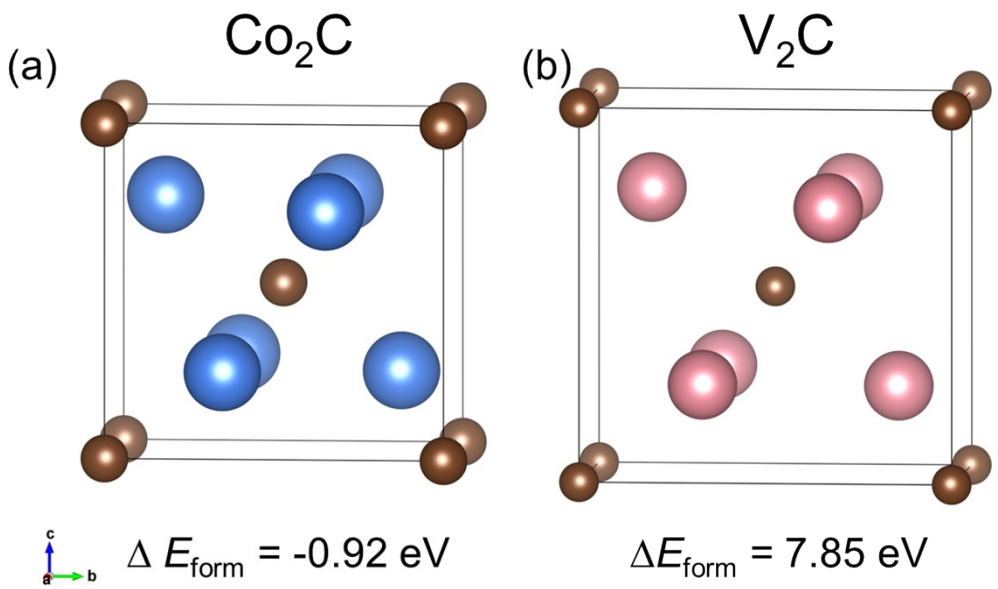

Fig. S11. Formation energy of (a) Co_2C and (b) V_2C.

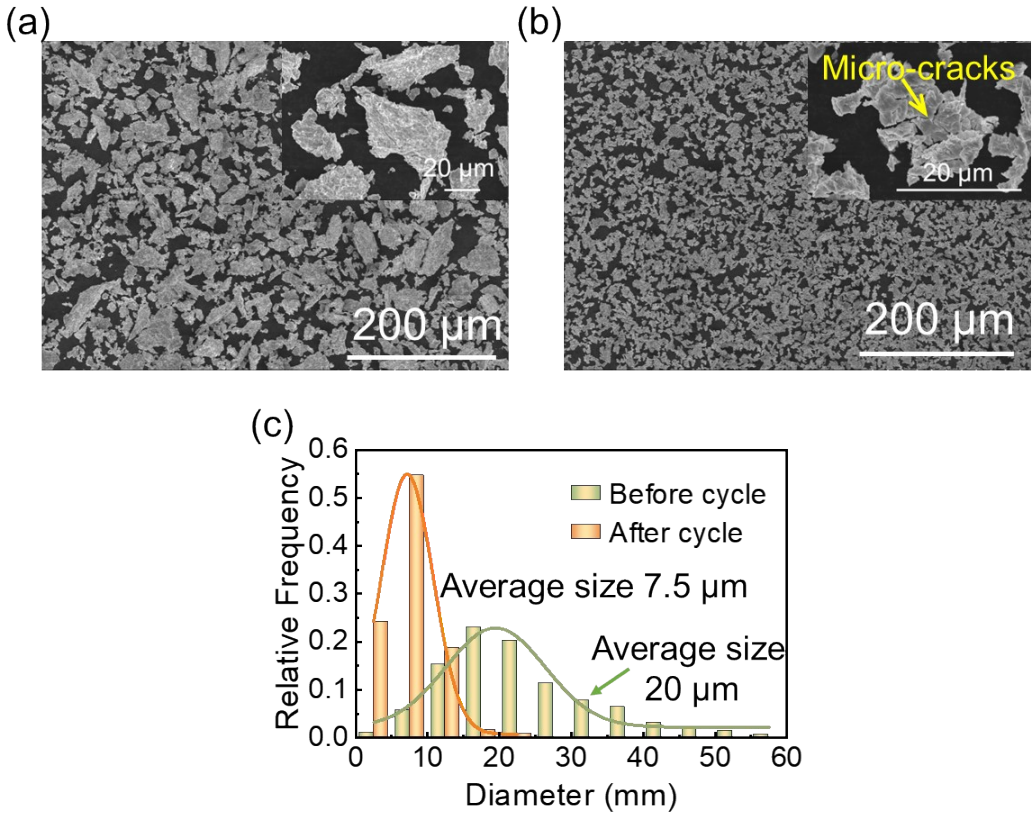

Fig. S12. SEM images of (a) before and (b) after cycle, and (c) corresponding particle size distribution statistics.

Supplementary Tables

Table S1. Thermodynamic characteristics for hydrogenation of $ZrCo_{1-x}V_x$ (x= 0, 0.03, 0.1) alloy and their maximum hydrogen storage capacities.

Sample	P_a [a)] (bar)			ΔH	ΔS	C_{max} [b)]
	250 °C	300 °C	350 °C	(kJ/mol H_2)	(J/K·mol H_2)	(wt%)
x = 0	0.066	0.171	0.481	-90.76	-150.73	1.93
x = 0.01	0.061	0.155	0.363	-92.28	-152.64	1.96
x = 0.1	0.056	0.256	0.427	-89.04	-146.85	1.92

[a)] P_a represents the hydrogenation plateau pressure dehydrogenated sample.

[b)] C_{max} represents the saturated hydrogen storage capacity of the sample at 20°C.

Table S2. Geometric and electronic configuration parameters of CO adsorbed on the surface of ZrCo-based alloy.

Gas-ZrCo	C-O length (Å)	ΔE / eV	ICOHP(C-O) at E_f
CO-gas	1.1434	-	-20.3701
ZrCo-CO	1.3868	-2.1730	-10.3545
ZrCoV-CO	1.3603	-2.7597	-9.7117

References

1 W. Tian, Z. Jia, T. Peng, Z. Wang, Z. Gao, Z. Luo, X. Sun, H. Zhang, Y. Zhou, R. Feng, H. Yuan and H. Cui, *Int. J. Hydrog. Energy*, 2026, **218**, 154072.

2 T. Peng, Z. Gao, Z. Wang, X. Sun, H. Zhang, Y. Zhou, Z. Luo, Z. Jia, P. Song, S. Lu, H. Cui, W. Tian, R. Feng, L. Jin and H. Yuan, *J. Mater. Sci. Technol.*, 2026, **246**, 1-12.

3 E. Halpren, X. Yao, Z. W. Chen and C. V. Singh, *Acta Mater.*, 2024, **270**, 119841.

4 P. P. Zhou, X. Z. Xiao, X. Y. Zhu, Y. P. Chen, W. M. Lu, M. Y. Piao, Z. M. Cao, M. Lu, F. Fang, Z. N. Li, L. J. Jiang and L. X. Chen, *Energy Storage Mater.*, 2023, **63**, 102964.

5 J. B. Zhang, H. K. Zhang, S. T. Weng, R. H. Li, D. Lu, T. Deng, S. Q. Zhang, L. Lv, J. C. Qi, X. Z. Xiao, L. W. Fan, S. J. Geng, F. H. Wang, L. X. Chen, M. Noked, X. F. Wang and X. L. Fan, *Nat. Commun.*, 2023, **14**, 2211.

6 G. Kresse and J. Hafner, *Phys. Rev. B*, 1994, **49**, 14251-14269.

7 G. Kresse and D. Joubert, *Phys. Rev. B*, 1999, **59**, 1758-1775.

8 J. P. Perdew, K. Burke and M. Ernzerhof, *Phys. Rev. Lett.*, 1996, **77**, 3865-3868.

9 B. Zhang, B. Luo, G. Sang, H. Kou, P. Li and W. Luo, *Int. J. Hydrog. Energy*, 2026, **219**, 154103.

10 B. Zhang, B. Luo, W. Luo, L. Zhou, H. Kou, P. Li and G. Sang, *Int. J. Hydrog. Energy*, 2024, **86**, 899-912.

11 D. Chattaraj, N. Kumar, P. Ghosh, C. Majumder and S. Dash, *Appl. Surf. Sci.*, 2017, **422**, 394-405.

12 J. P. Bi, P. P. Zhou, W. Jiang, H. Q. Kou, T. Tang, Y. J. Zhang, Y. Liu, Q. W. Zhou, Y. X. Yao, Y. Zhang, M. Yang, L. X. Chen and X. Z. Xiao, *Adv. Sci.*, 2024, **11**, 2408522.

13 R. Dronskowski and P. E. Blochl, *J. Phys. Chem.*, 1993, **97**, 8617-8624.

14 V. L. Deringer, A. L. Tchougréeff and R. Dronskowski, *J. Phys. Chem. A*, 2011, **115**, 5461-5466.